

Spectral-radiometric differentiation of non-photosynthetic vegetation and soil within Landsat and Sentinel 2 wavebands

Jie Dai, Dar Roberts, Philip Dennison & Douglas Stow

To cite this article: Jie Dai, Dar Roberts, Philip Dennison & Douglas Stow (2018) Spectral-radiometric differentiation of non-photosynthetic vegetation and soil within Landsat and Sentinel 2 wavebands, *Remote Sensing Letters*, 9:8, 733-742, DOI: [10.1080/2150704X.2018.1470697](https://doi.org/10.1080/2150704X.2018.1470697)

To link to this article: <https://doi.org/10.1080/2150704X.2018.1470697>



Published online: 24 May 2018.



Submit your article to this journal [↗](#)



View related articles [↗](#)



View Crossmark data [↗](#)



Spectral-radiometric differentiation of non-photosynthetic vegetation and soil within Landsat and Sentinel 2 wavebands

Jie Dai^{a,b}, Dar Roberts^b, Philip Dennison^c and Douglas Stow^{id a}

^aDepartment of Geography, San Diego State University, San Diego, CA, USA; ^bDepartment of Geography, University of California, Santa Barbara, CA, USA; ^cDepartment of Geography, University of Utah, Salt Lake City, UT, USA

ABSTRACT

We explore the comprehensive differentiation of non-photosynthetic vegetation (NPV) and soil using Landsat and Sentinel 2 wavebands through a spectral library approach. NPV and soil spectra from online spectral libraries and an Airborne Visible Infrared Imaging Spectrometer (AVIRIS) scene were convolved to Landsat 5 Thematic Mapper (TM), Landsat 8 Operational Land Imager (OLI), and Sentinel 2 bands. Several spectral-radiometric measurements, including the spectral reflectance of analogous Landsat and Sentinel bands, and a suite of spectral indices were tested for the separation of NPV and soil. Reflectance of individual bands is similar between the two categories, and vegetation indices such as Normalized Difference Vegetation Index (NDVI) and the Soil Adjusted Vegetation Index (SAVI) are incapable of such differentiation. For both reference and image spectra, the normalized difference tillage index (NDTI) based on the two short-wave infrared bands of Landsat and Sentinel instruments performed best among all spectral measurements. Classification results suggest an NDTI value of 0.1 to be a general threshold for separating NPV and soil, with higher values associated with NPV. Further tests based on AVIRIS-convolved imagery show that NDTI can dichotomize NPV and soil if either fractional cover is no less than 50%.

ARTICLE HISTORY

Received 19 July 2017
Accepted 22 April 2018

1. Introduction

1.1. Non-photosynthetic vegetation and its functions

Non-photosynthetic vegetation (NPV) usually refers to any vegetation components that do not photosynthesize (Roberts, Adams, and Smith 1993). These include both living parts like branches or stems, and dead portions, such as crop residues or fallen leaves. Okin (2007) made a distinction between litter from other NPV, based on the connection of a vegetation component to a rooted plant, and argued that litter has different structures and ecological functions. Nevertheless, they are similar in spectral and

chemical characteristics. In this study, we use the term NPV to represent all non-photosynthetic components of the vegetation.

NPV plays important roles in terrestrial ecosystems, with living NPV transporting nutrients and water from soil to the whole plant, and senesced NPV, or litter, connecting the life cycle between green vegetation and soil (Riaz et al. 2012). Litter will eventually decompose into soil, adding organic matter and nutrients to the ground (Henry, Brizgys, and Field 2008). Well-distributed NPV can buffer between soil and the atmosphere, reducing soil erosion, increasing moisture retention, and balancing ground surface temperatures (Deutsch, Bork, and Williams 2010). Increased levels of NPV can also increase the risk of wildfire (Roberts et al. 2006). The presence of NPV is not always beneficial, for it can attenuate sunlight, thus hindering the growth of understory vegetation (Jackson et al. 2006).

1.2. Spectral similarity between NPV and soil

NPV and soil exhibit similar spectral signatures, with no unique spectral features in the visible and near infrared (VNIR) wavelengths (Roberts, Adams, and Smith 1993). In the transition wavelength zone (680–780 nm) between the red and NIR, slopes of the spectral reflectance curves are usually greater for NPV than soil. However, the slope magnitudes are also sensitive to moisture and decomposition conditions (Nagler, Daughtry, and Goward 2000).

In the shortwave infrared wavelength region of the spectrum (SWIR2: 2.1–2.4 μm), NPV and soil show unique spectral derivatives signatures (Asner and Lobell 2000). Leveraging the spectral dip at 2.1 μm and the relative shoulders at 2.0 μm and 2.2 μm , the Cellulose Absorption Index (CAI) is an effective indicator of NPV (Nagler, Daughtry, and Goward 2000). But for CAI to work, image data covering these specific, narrow bands must be collected. Commonly available broadband multispectral sensors like those on Landsat satellites do not spectrally resolve these narrow wavelength features.

Previous efforts concerning broadband multispectral imagery have focused on the two SWIR bands. Both the Simple Tillage Index (STI) and Normalized Difference Tillage Index (NDTI) based on Landsat Thematic Mapper (TM) Band 5 and 7 were shown by Van Deventer et al. (1997) to effectively dichotomize between agricultural lands of conservative (more crop residue) and conventional (less crop residue) tillage, with a prediction accuracy of 89%. Guerschman et al. (2009) provides an empirical estimation of STI based on CAI and NDVI calculated from Hyperion and Hyperion-convolved MODIS data. In this sense, CAI can be retrieved through linear combination of STI and NDVI. Together with NDVI, STI has also been applied in spectral mixture analyses to identify potential NPV endmembers with different levels of successes in identifying NPV fraction covers in arid and semiarid ecosystems (Hill 2013; Smith, Hill, and Zhang 2015; Hill et al. 2017).

Given the relatively rare availability of imaging spectrometry in most areas of the world, and the tremendous temporal and spatial coverage of broadband multispectral imagery, the objective of this Letter is to differentiate NPV from soil cover in Landsat TM, Operational Land Imager (OLI) and Sentinel 2 multispectral data through a spectral library approach, and to determine which spectral measurements might be promising for distinguishing and quantifying these land cover types. We also attempt to determine at what fractional levels of NPV and soil the most effective spectral metrics are capable of distinguishing.

2. Data and methods

Laboratory/ground-measured NPV and soil spectra were acquired from two online sources. In the Jet Propulsion Laboratory (JPL) ASTER Spectral library (Baldrige et al. 2009, <http://speclib.jpl.nasa.gov>), 41 soil spectra and one dead grass spectrum were available in the visible through SWIR wavelength region 0.4 to 2.5 μm . Another 25 NPV spectra were obtained from the USGS Spectral Library (Kokaly, Clark, and Swayze et al. 2017, <http://speclab.cr.usgs.gov/spectral-lib.html>).

Apart from the reference spectra, supplementary image spectra were extracted from an Airborne Visible Infrared Imaging Spectrometer (AVIRIS) scene. With a 7.5 m spatial resolution, this scene was acquired over Santa Barbara, California on 19 July 2011 (Figure 1). Atmospheric correction and spectral reflectance retrieval was performed with ATCOR-4 radiation transfer modeling software (Richter and Schlaepfer 2002). Only the spectra of pixels with 75% or more coverage by one single land cover type were considered for the spectral library. For processing details and the development of spectral library please see Roberts et al. (2015). The image spectral library was generated following the basic procedures in Roth, Dennison, and Roberts (2012).

All NPV and soil spectra were convolved to Landsat 5 TM, Landsat 8 OLI and Sentinel 2 bands with the spectral resampling tool in ENVI image analysis software. Spectral separability of NPV and soil was evaluated with spectral reflectance for individual VNIR and SWIR bands (TM Bands 1–5 and 7; OLI Bands 1–7; Sentinel 2 Bands 1-8A, 11, and 12), and a suite of spectral indices (Table 1). The performance of each individual measurement was examined through exploratory statistics, and promising ones were further evaluated by the Receiver Operating Characteristic (ROC) curve in the R software package (Robin et al. 2011). ROC curve is a common practice of examining the separability of a binary classifier, by plotting the true positive rate against the false positive rate. Assessing results can be identified from Area under the Curve (AUC) values, where an AUC of 1 indicates perfect separation.

3. Results

3.1. Reference spectra

We identified a total of 41 soil and 26 NPV reference spectra, with explanatory statistics provided as following (Figure 2). Spectral reflectance convolved to Landsat and Sentinel 2 bands are mostly similar for NPV and soil. Although soil reflectance in SWIR2 (Landsat



Figure 1. False colour AVIRIS three-band composite for a study area in Santa Barbara and Goleta, California, USA. Red: 1.65 μm ; Green: 0.83 μm ; Blue: 0.68 μm .

Table 1. Spectral indices tested in this study.

Spectral Indices	References
Normalized Difference Vegetation Index NDVI = (NIR - R)/(NIR + R)	Rouse et al. (1973)
Soil-Adjusted Vegetation Index SAVI = (1.5NIR - R)/(NIR + R + 0.5)	Huete (1988)
Vegetation Index Green Vlg = (G - R)/(G + R)	Gitelson et al. (2002)
Simple Ratio Vegetation Index SRVI = NIR/R	Jordan (1969)
Normalized Difference Moisture Index NDMI = (NIR - SWIR1)/(NIR + SWIR1)	Hunt and Rock (1989)
Normalized Burn Ratio NBR = (NIR - SWIR2)/(NIR + SWIR2)	Key and Benson (2003)
Normalized Difference Senescent Vegetation Index NDSVI = (SWIR1 - R)/(SWIR1 + R)	Qi and Wallace (2002)
Dead Fuel Index DFI = 100(1 - SWIR2/SWIR1)(R/NIR)	Cao et al. (2010)
Normalized Difference Tillage Index NDTI = (SWIR1-SWIR2)/(SWIR1+SWIR2)	Van Deventer et al. (1997)

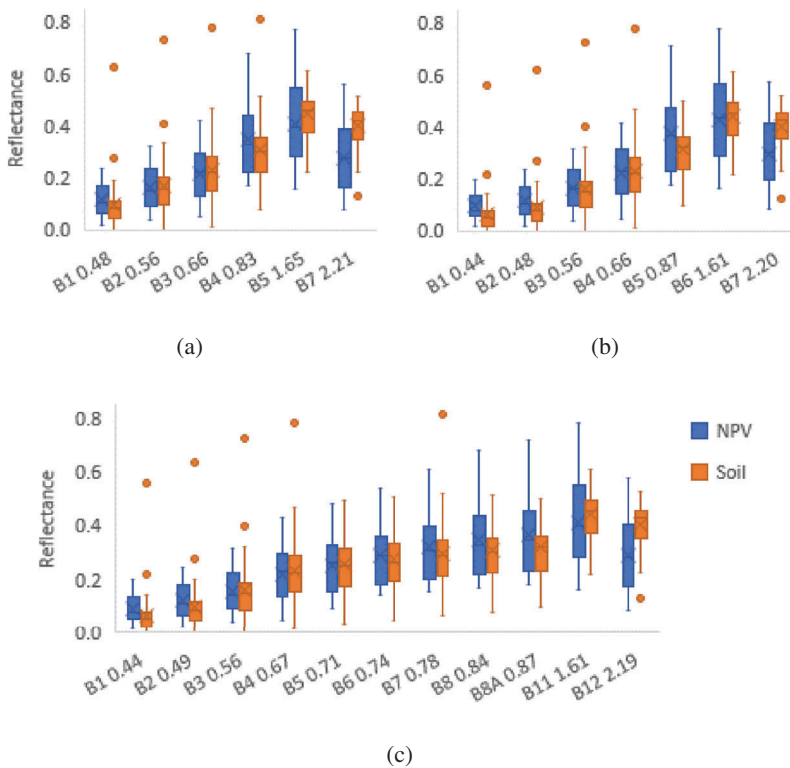


Figure 2. Boxplots of reference NPV and soil spectral reflectance convolved to (a) Landsat TM bands, (b) Landsat OLI bands and (c) Sentinel 2 bands. 'B1 0.48' means Band 1 reflectance centred at 0.48 μm wavelength.

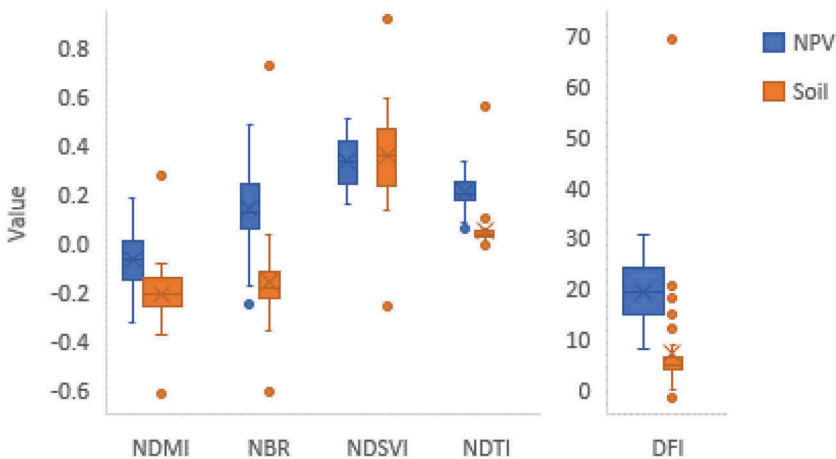


Figure 3. Boxplots of indices for reference NPV and soil spectra in Landsat TM bands.

B7; Sentinel 2 B12) is generally higher than NPV, the difference is not sufficiently prominent to warrant using this band alone as a discriminating variable for NPV and soil.

Simple ratio vegetation index, SRVI, and normalized vegetation index values, such as NDVI, SAVI, and Vig, are quite similar for soil and NPV making it difficult to separate them, and they are not analysed here. Four other spectral indices, NDMI, NBR, NDTI, and DFI, exhibit different values for NPV and soil (Figure 3). The indices' differences between NPV and soil are similar among spectra convolved to Landsat and Sentinel 2 bands. The above-mentioned four measures, plus NDSVI, were further evaluated by ROC curves. Among these five indices, NDTI has the highest AUC of 0.96 (Table 2), indicating its superiority in differentiating NPV and soil.

3.2. Image spectra

A total of 2551 NPV spectra and 1397 soil spectra were extracted from the AVIRIS scene. The same procedure was applied to the image spectra as with the reference spectra. However, only the five indices listed in Table 2 were examined. Again, NDTI outperformed the other indices, with an AUC value extremely close to 1 and only three spectra misclassified out of approximately four thousand NPV/soil spectra, indicating its ability to differentiate almost all NPV and soil spectra (Table 3). Most NPV spectra have NDTI values between 0.10 and 0.25, while soil samples are mostly negative or around zero.

ROC curve analysis also suggest optimal NDTI thresholds for separating NPV from soil (Table 4). In reference spectra convolved to Landsat and Sentinel 2 bands, the thresholds were set to around 0.125. In image spectra, the NDTI thresholds are 0.0846, 0.0623, and 0.0609 for Landsat TM, OLI, and Sentinel 2, respectively.

Table 2. AUC of spectral indices for reference spectra in Landsat and Sentinel 2 bands.

	NDMI	NBR	NDSVI	NDTI	DFI
TM	0.8302	0.9184	0.545	0.9662	0.9418
OLI	0.8293	0.9174	0.5422	0.9634	0.9343
Sentinel 2	0.8161	0.9137	0.5249	0.9634	0.9390

Table 3. AUC of spectral indices for image spectra in Landsat and Sentinel 2 bands.

	NDMI	NBR	NDSVI	NDTI	DFI
TM	0.8170	0.9276	0.8972	1	0.9998
OLI	0.7840	0.9380	0.8981	1	0.9999
Sentinel 2	0.8258	0.8955	0.8979	1	0.9999

Table 4. Optimal NDTI thresholds as well as the true and false positive rates.

	Reference spectra			Image spectra		
	TM	OLI	Sentinel 2	TM	OLI	Sentinel 2
Threshold	0.1236	0.1273	0.1256	0.0846	0.0623	0.0609
True positive rate	0.9231	0.9600	0.9600	0.9996	0.9992	0.9992
False positive rate	0.0769	0.0769	0.0769	0.0008	0.0004	0.0004

4. Discussion

The key contribution of this Letter is determining which Landsat/Sentinel 2 spectral index best differentiate NPV from soil. NDTI performed best among all spectral measurements for both reference and image spectra.

In only a few cases were spectra misclassified (Table 5). In reference data, the two misclassified soil spectra exhibited unique spectral features compared to other soil samples (Figure 4). White gypsum dune sand (100% sand) is very bright in the VNIR, but the reflectance curve drops sharply in the SWIR. This sample can be readily separated with NPV using other spectral measurements like reflectance in visible wavelength, where most NPV is darker. The other misclassified soil sample, dark yellowish brown silty clay, exhibits a steeper slope in spectral curve between SWIR Band 1 (TM Band 5, OLI Band 6, Sentinel 2 Band 11) and SWIR Band 2 (TM/OLI Band 7, Sentinel 2 Band 12) than other soil samples. Dead willow spectra do not show a prominent lignin and cellulose absorption feature in the 2.1 μm wavelength. Besides, the differences of the two SWIR bands are not prominent in mature brown cheatgrass (*Bromus tectorum*) and smooth cordgrass (*Spartina alterniflora*). Thus, NDTI value for the dark yellowish brown silty clay is greater than or similar to that for the three NPV spectra mentioned above.

To further validate the performance of NDTI, we randomly selected 100 validation polygons in the AVIRIS imagery. For details, please see Roberts et al. (2015). We utilized the fraction maps generated from multiple endmember spectral mixture analysis (MESMA; Roberts et al. 1998) in Roberts et al. (2017) to guide our validation work. First, we extracted all spectra in the validation polygons. We then classified validation spectra into six categories, per endmember (NPV/soil) fractions. For example, all pixels with NPV fractions greater than 0.75 would be aggregated into category one. Then pixels with NPV fractions between 0.70 and 0.75 would be placed in category two, 0.65 to 0.70 to category three, etc., and at last, 0.50 to 0.55 to category six. The same

Table 5. NDTI values of misclassified NPV and soil in reference spectra.

		TM	OLI	Sentinel 2
NPV	Mature brown cheatgrass (<i>Bromus tectorum</i>)	0.0599	0.0397	0.0397
	Smooth cordgrass (<i>Spartina alterniflora</i>)	0.0859	0.0722	0.0714
	Dead Willow	0.1263	0.1289	0.1279
Soil	Grey stoney coarse sandy soil	0.1209	0.1139	0.1123
	Dark yellowish brown silty clay	0.1336	0.1259	0.1233
	White gypsum dune sand	0.5609	0.6097	0.6118

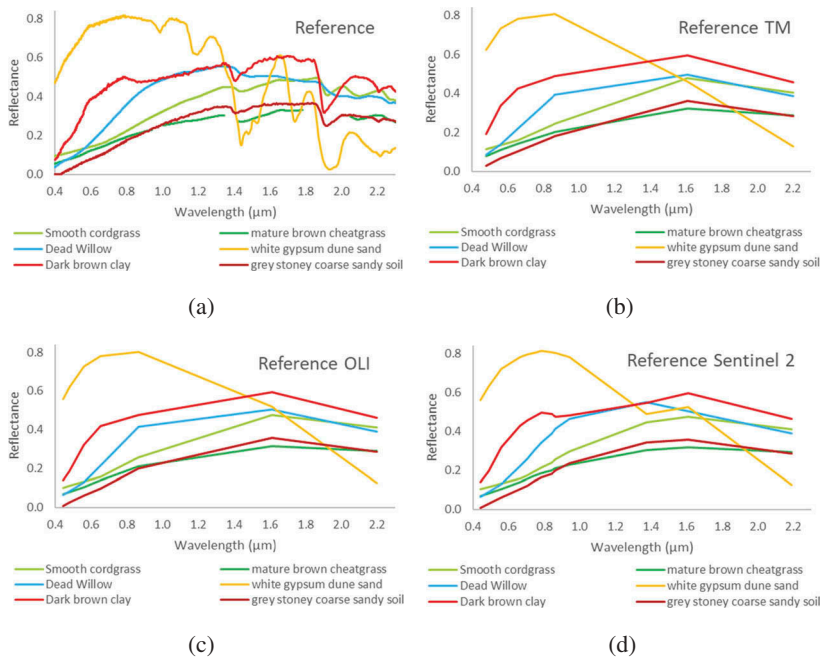


Figure 4. Continuous and convolved spectrum of misclassified NPV and soil samples in reference spectra (a), Landsat TM wavebands (b), OLI wavebands (c), and Sentinel 2 wavebands (d).

procedure was conducted for soil fractions. In the next step, we compare NPV and soil pixels from the same category through ROC curves. The comparison in category one indicated how well NDTI performed for pixels dominated by NPV/soil (fraction ≥ 0.75). For the other categories, the purpose of the validation was to identify in what fractions NDTI would fail as an effective indicator. Note that NPV and soil may not be the only endmembers in the pixel, and other endmember types, such as green vegetation, rock, pavement, etc., may also be present, although NPV or soil occupy no less than half of the spatial extent (with fraction ≥ 0.50). If NDTI can still routinely distinguish NPV from soil under these circumstances, we are confident that it can do so in NPV-soil-only-mixture situations. The validation results suggest that in almost all cases, NDTI generated AUC values were higher than 0.9, indicating its excellence in differentiating NPV and soil (Table 6).

We suggest two major reasons why NDTI performed better than other spectral indices. First, the most prominent spectral difference between NPV and soil is the cellulose absorption feature in SWIR 2 wavelengths. When convolved to broadband multispectral sensor, the absorption will produce the descending curve between the two SWIR bands, the basis in which NDTI was developed (Figure 2). In other words, NDTI better captures the spectral difference between NPV and soil than other broadband indices tested in this study. Second, the distribution of NDTI values for soil is much tighter than any other index (Figure 3). Less variance is helpful to generate better AUC values in ROC analysis.

Although NDTI performed well in this study, several issues should be taken into consideration. First, the available image spectra solely represented those from

Table 6. Sample size (# pixels) of validation NPV and soil spectra, as well as the AUC values of ROC curves (with suggested NDTI thresholds in parentheses).

Category	NPV or soil Fractions	Sample (# pixels)		AUC values and NDTI thresholds		
		NPV	Soil	TM	OLI	Sentinel 2
1	[0.75, 1.00]	529	369	0.9735(0.1045)	0.9702(0.0758)	0.9706(0.0730)
2	[0.70, 0.75]	62	103	0.9081(0.1546)	0.9085(0.1323)	0.9120(0.1102)
3	[0.65, 0.70]	91	123	0.9457(0.1072)	0.9386(0.0973)	0.9428(0.0968)
4	[0.60, 0.65]	102	107	0.9123(0.1008)	0.8966(0.0897)	0.9010(0.0874)
5	[0.55, 0.60]	111	129	0.9207(0.1227)	0.9113(0.0853)	0.9118(0.0973)
6	[0.50, 0.55]	129	220	0.9258(0.0856)	0.9111(0.0701)	0.9133(0.0687)

Mediterranean-type landscapes, and most spectra are in dry condition at least in the top layer. Ideally, NPV and soil spectra of all kinds from different landscape, ecosystem types and weather conditions should be tested for a comprehensive separation. Besides, we only considered situations where NPV or soil fractions were more than 0.5. In a more complex mixture where more endmember types are involved and their fractions are more even, the detection limits may be very different. Nevertheless, the purpose of this study is to highlight the potential of NDTI in differentiating NPV and soil in Landsat and Sentinel 2 wavebands, and we encourage further testing based on other spectra sources from other ecosystem types.

Funding

This work was funded by National Aeronautics and Space Administration grant id 17-EARTH17F-337.

ORCID

Douglas Stow  <http://orcid.org/0000-0001-5246-7073>

References

- Asner, G. P., and D. B. Lobell. 2000. "A Biogeophysical Approach for Automated SWIR Unmixing of Soils and Vegetation." *Remote Sensing of Environment* 74: 99–112. doi:10.1016/S0034-4257(00)00126-7.
- Baldrige, A. M., S. J. Hook, C. I. Grove, and G. Rivera. 2009. "The ASTER Spectral Library Version 2.0." *Remote Sensing of Environment* 113: 711–715. doi:10.1016/j.rse.2008.11.007.
- Cao, X., J. Chen, B. Matsushita, and H. Imura. 2010. "Developing a MODIS-based Index to Discriminate Dead Fuel from Photosynthetic Vegetation and Soil Background in the Asian Steppe Area." *International Journal of Remote Sensing* 31: 1589–1604. doi:10.1080/01431160903475274.
- Deutsch, E. S., E. W. Bork, and W. D. Williams. 2010. "Separation of Grassland Litter and Ecosite Influences on Seasonal Soil Moisture and Plant Growth Dynamics." *Plant Ecology* 209: 135–145. doi:10.1007/s11258-010-9729-6.
- Gitelson, A. A., Y. J. Kaufman, R. Stark, and D. Rundquist. 2002. "Novel Algorithms for Remote Estimation of Vegetation Fraction." *Remote Sensing of Environment* 80: 76–87. doi:10.1016/S0034-4257(01)00289-9.
- Guerschman, J. P., M. J. Hill, L. J. Renzullo, D. J. Barrett, A. S. Marks, and E. J. Botha. 2009. "Estimating Fractional Cover of Photosynthetic Vegetation, Non-Photosynthetic Vegetation

- and Bare Soil in the Australian Tropical Savanna Region Upscaling the EO-1 Hyperion and MODIS Sensors." *Remote Sensing of Environment* 113: 928–945. doi:10.1016/j.rse.2009.01.006.
- Henry, H. A. L., K. Brizgys, and C. B. Field. 2008. "Litter Decomposition in a California Annual Grassland: Interactions between Photodegradation and Litter Layer Thickness." *Ecosystems* 11: 545–554. doi:10.1007/s10021-008-9141-4.
- Hill, M. J. 2013. "Vegetation Index Suites as Indicators of Vegetation State in Grassland and Savannah: An Analysis with Simulated SENTINEL 2 Data for a North American Transect." *Remote Sensing of Environment* 137: 94–111. doi:10.1016/j.rse.2013.06.004.
- Hill, M. J., Q. Zhou, Q. Sun, C. B. Schaaf, and M. Palace. 2017. "Relationships between Vegetation Indices, Fractional Cover Retrievals and the Structure and Composition of Brazilian Cerrado Natural Vegetation." *International Journal of Remote Sensing* 38: 874–905. doi:10.1080/01431161.2016.1271959.
- Huete, A. R. 1988. "A Soil-Adjusted Vegetation Index (SAVI)." *Remote Sensing of Environment* 25: 295–309. doi:10.1016/0034-4257(88)90106-X.
- Hunt Jr., E. R., and B. N. Rock. 1989. "Detection of Changes in Leaf Water Content Using Near- and Middle-Infrared Reflectances." *Remote Sensing of Environment* 30: 43–54. doi:10.1016/0034-4257(89)90046-1.
- Jackson, R. D., B. Allen-Diaz, L. G. Oates, and K. W. Tate. 2006. "Spring-Water Nitrate Increased with Removal of Livestock Grazing in a California Oak Savanna." *Ecosystems* 9: 254–267. doi:10.1007/s10021-005-0166-7.
- Jordan, C. F. 1969. "Derivation of Leaf-Area Index from Quality of Light on the Forest Floor." *Ecology* 50: 663–666. doi:10.2307/1936256.
- Key, C. H., and N. C. Benson. 2003. *The Normalized Burn Ratio (NBR): A Landsat TM Radiometric Measure of Burn Severity*. Washington, DC: U.S. Geological Survey Northern Rocky Mountain Science Center. U.S. Department of the Interior.
- Kokaly, R. F., R. N. Clark, G. A. Swayze, K. E. Livo, T. M. Hoefen, N. C. Pearson, R. A. Wise, W. M., et al. 2017. "USGS Spectral Library Version 7." *U.S. Geological Survey, Data Series* 1035: 61.
- Nagler, P. L., C. S. T. Daughtry, and S. N. Goward. 2000. "Plant Litter and Soil Reflectance." *Remote Sensing of Environment* 71: 207–215. doi:10.1016/S0034-4257(99)00082-6.
- Okin, G. S. 2007. "Relative Spectral Mixture Analysis – A Multitemporal Index of Total Vegetation Cover." *Remote Sensing of Environment* 106: 467–479. doi:10.1016/j.rse.2006.09.018.
- Qi, J., and O. Wallace. 2002. "Biophysical Attributes Estimation from Satellite Images in Arid Regions." In *2002 IEEE International on Geoscience and Remote Sensing Symposium, 2002. IGARSS'02*. Toronto, Ontario, Canada. doi:10.1109/IGARSS.2002.1026426.
- Riaz, M., I. A. Mian, A. Bhatti, and M. S. Cresser. 2012. "An Exploration of How Litter Controls Drainage Water DIN, DON and DOC Dynamics in Freely Draining Acid Grassland Soils." *Biogeochemistry* 107: 165–185. doi:10.1007/s10533-010-9544-0.
- Richter, R., and D. Schlaepfer. 2002. "Geo-Atmospheric Processing of Airborne Imaging Spectrometry Data. Part 2: Atmospheric/Topographic Correction." *International Journal of Remote Sensing* 23: 37–41. doi:10.1080/01431160110115834.
- Roberts, D. A., J. B. Adams, and M. O. Smith. 1993. "Green Vegetation, Non-Photosynthetic Vegetation and Soils in AVIRIS Data." *Remote Sensing of Environment* 44: 255–269. doi:10.1016/0034-4257(93)90020-X.
- Roberts, D. A., M. Alonzo, E. B. Wetherley, K. L. Dudley, and P. E. Dennison. 2017. "Multiscale Analysis of Urban Areas Using Mixing Models." In *Integrated Scale in Remote Sensing and GIScience Applications*, edited by D. A. Quattrochi et al., 247–282. New York: CRC Press.
- Roberts, D. A., P. E. Dennison, S. Peterson, S. Sweeney, and J. Rechel. 2006. "Evaluation of Airborne Visible/Infrared Imaging Spectrometer (AVIRIS) and Moderate Resolution Imaging Spectrometer (MODIS) Measures of Live Fuel Moisture and Fuel Condition in a Shrubland Ecosystem in Southern California." *Journal of Geophysical Research: Biogeosciences* 111: G0402. doi:10.1029/2005JG000113.
- Roberts, D. A., P. E. Dennison, K. L. Roth, K. Dudley, and G. Hulley. 2015. "Relationships between Dominant Plant Species, Fractional Cover and Land Surface Temperature in a Mediterranean Ecosystem." *Remote Sensing of Environment* 167: 152–167. doi:10.1016/j.rse.2015.01.026.

- Roberts, D. A., M. Gardner, R. Church, S. Ustin, G. Scheer, and R. O. Green. 1998. "Mapping Chaparral in the Santa Monica Mountains Using Multiple Endmember Spectral Mixture Models." *Remote Sensing of Environment* 65: 267–279. doi:10.1016/S0034-4257(98)00037-6.
- Robin, X., N. Turck, A. Hainard, N. Tiberti, F. Lisacek, J.-C. Sanchez, and M. Müller. 2011. "pROC: An Open-Source Package for R and S+ to Analyze and Compare ROC Curves." *BMC Bioinformatics* 12: 77. doi:10.1186/1471-2105-12-77.
- Roth, K. L., P. E. Dennison, and D. A. Roberts. 2012. "Comparing Endmember Selection Techniques for Accurate Mapping of Plant Species and Land Cover Using Imaging Spectrometer Data." *Remote Sensing of Environment* 127: 139–152. doi:10.1016/j.rse.2012.08.030.
- Rouse, J. W., R. H. Hass, J. A. Schell, and D. W. Deering. 1973. "Monitoring Vegetation Systems in the Great Plains with ERTS." In *Proceedings of the Third ERTS Symposium*, edited by S. C. Freden et al., 309–317. Washington, DC: NASA.
- Smith, A. M., M. J. Hill, and Y. Zhang. 2015. "Estimating Ground Cover in the Mixed Prairie Grassland of Southern Alberta Using Vegetation Indices Related to Physiological Function." *Canadian Journal of Remote Sensing* 41: 51–66. doi:10.1080/07038992.2015.1042101.
- Van Deventer, A. P., A. D. Ward, P. H. Gowda, and J. G. Lyon. 1997. "Using Thematic Mapper Data to Identify Contrasting Soil Plains and Tillage Practices." *Photogrammetric Engineering & Remote Sensing* 63: 87–93.